Optics and Lasers in Engineering 158 (2022) 107173

Contents lists available at ScienceDirect

Optics and Lasers in Engineering

journal homepage: www.elsevier.com/locate/optlaseng

A microfluidic system for analysis of electrochemical processing using a highly sensitive optical fiber microcavity

Andrzej Krześniak[a,1], Tomasz Gabler[b,1], Monika Janik[b,c], Marcin Koba[b,d], Martin Jönsson-Niedziółka[a,*], Mateusz Śmietana[b,*]

[a] Polish Academy of Sciences, Institute of Physical Chemistry, Kasprzaka 44/52, Warsaw 01-224, Poland
[b] Institute of Microelectronics and Optoelectronics, Warsaw University of Technology, Koszykowa 75, Warsaw 00-662, Poland
[c] Department of Metrology and Optoelectronics, Gdańsk University of Technology, Narutowicza 11/12, Gdańsk 80-233, Poland
[d] National Institute of Telecommunications, Szachowa 1, Warsaw 04-894, Poland

ARTICLE INFO

Keywords:
Microfluidics
Optical fiber sensor
Refractive index sensing
Mach-Zehnder interferometer
Electrochemistry

ABSTRACT

Microfluidics provide unique possibilities to control tiny volumes of liquids and their composition. In this work we combined a microfluidic system with a microcavity in-line Mach-Zehnder interferometer (μIMZI) induced in the side surface of a single-mode optical fiber using a femtosecond laser micromachining. The μIMZI shows capability for investigating optical properties of volumes down to picoliters with an exceptionally high refractive index sensitivity. Here we report numerical analysis and experimental results that show that when the μIMZI is incorporated with the microfluidic system the measurements can be performed with sensitivity exceeding 14,000 nm/RIU which is similar to measurements done under static conditions. In a flow injection system, we show the influence of flow rate and injection volume on the response, and that the orientation of the cavity versus the flow direction has only a minor impact on the results. Finally, we have supported the system by band electrodes making it possible to induce redox reactions in the microchannel to detect the flowing products of the reactions optically. It has been found that thanks to the high sensitivity of the μIMZI the products of the reactions can be clearly detected both electrochemically and optically even when the only part of the flowing redox probe is oxidized at the band electrode. The capability for monitoring the products was shown for a standard redox probe, potassium ferricyanide, as well as for the neurotransmitter dopamine. This work shows that the proposed solution may offer highly sensitive optical measurements, even when the chemical reactions are not effective in the whole volume of the system.

1. Introduction

Microfluidics is a multidisciplinary field of studies aiming to manipulate fluids that are geometrically constrained to a small scale at which surface forces dominate over volumetric forces. Research on microfluidics started in the 1980s and since then it has been widely developed in various branches of science [1]. Small size is a defining feature of microfluidic devices, but there are other valuable advantages of moving from the macro to microscale. The small volumes (micro to picoliters) associated with microfluidics results in diffusion being an important mode of mass transport [2,3]. Because of that, laminar flow regimes are fully developed, and fluid mixing occurs in a controllable fashion. The laminar nature of flow in turn ensures that particle or fluid motion is well-defined and can be engineered towards a particular purpose. For example, the flow may be designed to direct and distribute a stream of molecules to specific streamlines based on their molecular structure, e.g., surface-specific antigens, or depending on their physical (size) or electrical properties [2].

The large surface-area-to-volume ratios of the fluids ensure thermal homogeneity across the stream and rapid heat transfer between the device and the fluid. This advantage helps maintain uniform reaction conditions that are particularly important in chemical and biological systems [4]. For these reasons, scaling such systems down to nanoliter or picoliter volumes can fundamentally improve the sensitivity of conducted analysis, simultaneously limit the reagent volume, and therefore reduce final cost of the analysis.

To develop an operational microfluidic-based sensing system, the microfluidic technology needs to be integrated with, e.g. electrical or optical devices, that are required for interrogating the obtained outcomes. Although the microfluidic systems themselves are usually highly miniaturized, most of them still require support of external, bulky systems,

* Corresponding authors.
E-mail addresses: martinj@ichf.edu.pl (M. Jönsson-Niedziółka), M.Smietana@elka.pw.edu.pl (M. Śmietana).
[1] These authors contributed equally to this work.

https://doi.org/10.1016/j.optlaseng.2022.107173
Received 20 March 2022; Received in revised form 15 June 2022; Accepted 26 June 2022
Available online 2 July 2022

such as a fluorescent microscope [5,6]. Therefore, a step ahead is to develop miniature interrogation subsystems, but still highly functional and compatible with microfluidics. To improve the sensing efficiency and tackle such challenges as portability and miniaturization of the whole system, optofluidic devices have been proposed where microfluidic (or nanofluidic) systems are integrated with optical sensing devices [7–10]. Such solutions provide conditions for direct interaction between the examined fluid and light, which is expected e.g., in the field of biochemical sensing [11]. Until now a variety of planar optical sensing solutions have been combined with microfluidics [11,12]. Nevertheless, the sensitivity of such systems to changes in optical properties of the fluids, such as their refractive index (RI), is often relatively low, i.e., when a spectral shift of a pattern is concerned, it reaches a level of tens up to hundreds of nm per refractive index unit (RIU). On top of sensitivity, a crucial issue is a proper integration and alignment of the optical components with microfluidic devices.

In parallel to planar optical sensing solutions, miniaturized, robust, portable, but most importantly highly sensitive approaches based on optical fibers have been proposed [13–16]. Such devices show several notable advantages over the planar ones. First, they are inexpensive thanks to the well-established fiber manufacturing technology. Moreover, they can easily couple light into microfluidic channels due to their similar size. Also, their immunity to electromagnetic interference and the possibility of remote measurements are additional advantages. In general, optical fibers may be integrated with microfluidics in three different ways. First, thanks to the microstructure of some fibers, they can serve as both light transmission medium and microfluidic channel, as it is in the case of, e.g., a hollow core fibers [17,18]. Second, by introduction of microstructuring processes such as those based on femtosecond (fs) laser micromachining or ion beam lithography creating lab-in-fiber systems [19,20]. Third, the most common method due to the flexibility in application of various types of sensors, is achieved by the integration of fiber-based sensors with extrinsic microfluidic channels. Interferometers [21], various gratings [22–24], micro/nano fibers [25,26], and nanocoated fibers (based on surface plasmon resonance [27] or lossy-mode resonance [28] effects) have been shown following this approach.

However, integration of the optical fiber sensor with the microfluidic system plays a crucial role during the sensing process. The way of introducing the analyte to the microchannels and efficiency of this process are especially important. Furthermore, the sensitivity of the sensor to external changes needs to be high enough to enable measurements of the analyte present in the microchannel. Volume of the analyte needed for the detection process is also important. It must be noted that some sensors, e.g., gratings [29], or lossy-mode resonance [28], need hundreds of microliters of samples per single analysis due to their size/length and inaccurately defined sensing area. Such volumes may be too large in the case of biological and chemical materials with limited availability or high cost. Furthermore, such elongated interaction volumes may also influence the distribution of the monitored analyte, thereby distorting the precision and increasing the limit of detection. This is especially problematic during monitoring and analyzing reactions/processes, where the overall efficiency is low. Moreover, it is worth mentioning that the sensitivity of evanescent wave-based devices is often intrinsically limited by the short penetration depth of light in the fluid at the device surface. This, in turn, strongly limits the applications of such sensing systems.

A Microcavity in-line Mach-Zehnder Interferometer (μIMZI) is an open cavity micromachined in the fiber cladding and partly into the fiber core. In this configuration, the microcavity splits incoming light into two parts, where one remains in the fiber core (reference beam), while the other one propagates through the cavity (sensing beam). The two beams interfere at the far sidewall of the cavity [30]. Due to the precise, one-step fabrication process, the platform is highly reproducible and provides a well-defined sensing area. The μIMZI with a diameter of a few tens of micrometers allows sub-nanoliter volumes of liquids to be investigated in a well-defined spot. Through direct light-analyte interaction, the sensitivity of the μIMZI regularly reaches over a dozen thousand nm/RIU [31] which makes it a perfect choice for bio- and chemo-sensing, especially when small volumes of analytes are considered. Although the μIMZI has been reported for different applications, such as bacteria detection [32,33] and real-time monitoring of isothermal DNA amplification [34], its integration with the extrinsic microfluidic channel has never been reported. Incorporation of the μIMZI in a microfluidic system may also be advantageous because it limits evaporation of the analyte and allows a more accurate way of handling a solution inside the microcavity as it can be easily exchanged. Moreover, due to limited exposure of the sensor to changes in environmental conditions, such as drying during the procedure, some additional effects possibly modifying the sensor surface and disturbing the measurements can be mitigated [35].

In this work, we integrate a μIMZI sensor as an element of a microfluidic system for real-time monitoring of chemical reactions products. In contrast to the work of Li et al. in [36], where the microfluidic channel was laser micromachined together with the microcavity inside an optical fiber, we have implemented an external microfluidic system capable of accommodating additional elements of the microsystem, such as electrodes. Thanks to that a multi-domain, optical and electrochemical (EC), μIMZI-based microfluidic system was developed and used for real-time monitoring of exchange between oxidized and reduced forms of a $K_4Fe(CN)_6$ / $K_3Fe(CN)_6$. In contrast to the sensing concept reported previously by our team in [37], where EC reactions were initiated directly in the cavity, we investigated the capability of the system for optical measurements of EC reactions taking place outside the cavity. Since the size of the cavity's sensing area is much smaller than other optical fiber sensors integrated with microfluidics investigated up until now, the liquid exchange in the cavity has been discussed theoretically and experimentally. The universality, high sensitivity, capability for further miniaturization, and possibility of combining the system with other devices make the μIMZI-based microfluidic system suitable for practical applications in biological and chemical research including drug discovery and development.

2. Materials and methods

2.1. Fabrication and optical measurements of the microcavities

Circular microcavities (54 μm diameter, 62.5 μm depth) were fabricated in the sidewall of standard Corning SMF28 fibers. The cladding and core diameters of the SMF28 fiber are 125 and 8.2 μm, respectively. The fabrication process starts is the middle, top point of the cladding side surface. The micromachining process was performed using an NKT Origami 10XP laser operating at a wavelength of 1030 nm. The fiber was irradiated by ca. 400 fs pulses. Fused silica glass shows very low absorption at 1030 nm, and therefore linear absorption of the laser radiation does not occur when the glass is irradiated by the laser beam [38]. The system worked with a repetition rate of 15 kHz. The laser beam was focused on the sample with a suitably designed micromachining setup based on a Newport mFab system. It was equipped with a 20x lens (NA = 0.30). The laser pulse energy was equal to 6 nJ. Fiber transmission was monitored during the process with an NKT Photonics SuperK COMPACT supercontinuum white light source and a Yokogawa AQ6370D optical spectrum analyzer. The fabrication process was controlled with an in-house developed software and takes about 30 min.

During initial testing the spectral response of the μIMZIs were measured in widest wavelength range available to us, from 1100 to 1700 nm, using a Yokogawa AQ6370B optical spectrum analyzer and a Leukos SM30 supercontinuum white light laser source. The refractive index sensitivity was measured by immersing the sensors in glycerine/water solutions with refractive index in the range n_D=1.33300–1.40100 RIU. The n_D of the solutions was determined using Rudolph J57 automatic refractometer. The transmission measurements were conducted at constant mechanical tension and temperature (25 °C).

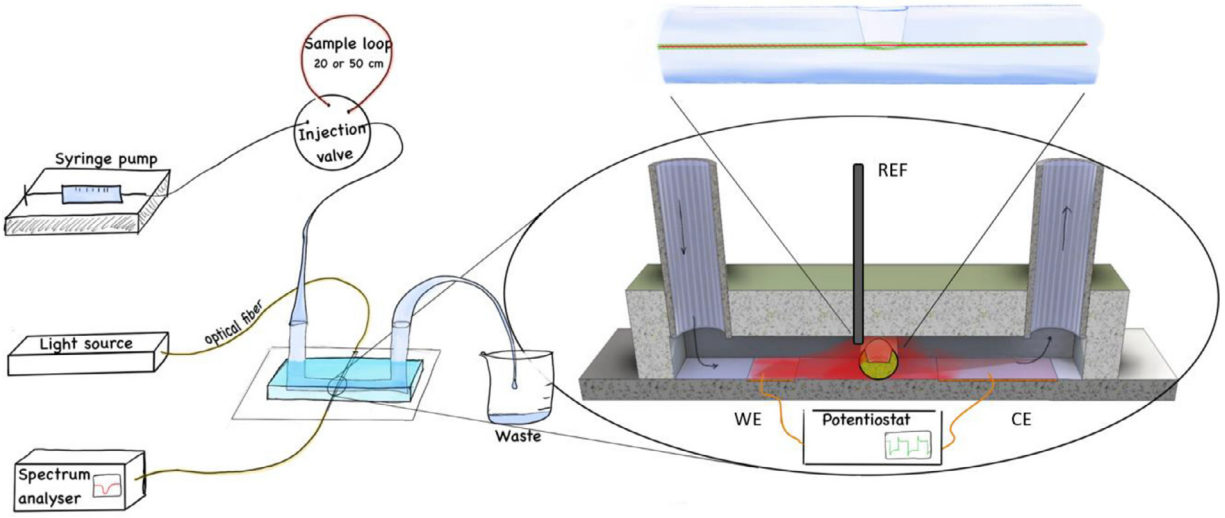

Fig. 1. Schematic representation of the experimental setup, with the optical fiber mounted perpendicular to the microchannel with the cavity inside the channel. Changes in composition are measured using a spectrum analyser.

2.2. Fabrication of microfluidic system

For fabrication of the microfluidic system glass slides (50 × 25 × 1.1 mm) coated with indium tin oxide (ITO) from Delta Technologies, Ltd. were used as a substrate. The electrodes were made by etching the ITO in a solution of $FeCl_3$ as described previously in [3]. First, the shape of the electrodes was defined by kapton tape cut using GCC LaserPro C180II Laser Engraver controlled by a computer program. The tape was used to mask the ITO electrodes during the etching process. The width of the working (WE) and counter electrode (CE) was 8 mm and 10 mm, respectively, to ensure that the half-reaction on the CE is not rate limiting. Next, the CE was covered with gold using a sputtering deposition method to increase its electrochemical activity. A 5 nm layer of Ti was used under the gold film to promote adhesion.

Next, for microchannel fabrication PDMS (Sylgard 184 Silicone, a two-part poly(dimethylsiloxane) elastomer from Dow Corning) was used. Firstly, a matrix for the channel was designed and printed in polylactic acid (PLA) using a 3D printer (Ultimaker 2+). Then, a microchannel was made by pouring the monomers of PDMS into the matrix and drying for 90 min at 65 °C. As a result, a 500 μm wide, 180 μm high, and 2 cm long microchannel was received. Holes for the liquid inlet and outlet, as well as the reference electrode were made in the PDMS using a biopsy punch. Finally, the optical fiber with the microcavity was installed between WE and CE and the PDMS as shown in Fig. 1. Since the fiber might rotate when installed we made numerical simulations to show that the orientation of the cavity has minor influence on the exchange of liquid (SI, Section 1).

2.3. Flow injection and electrochemical experiment

The electrochemical response of the sensor has been studied using a portable PalmSens4 potentiostat controlled to a computer equipped with PSTrace 5.6 software. A bare ITO electrode was used as working electrode, whereas ITO coated with gold served as counter electrode. An external Ag/AgCl electrode was used as a reference electrode. Copper tape was used to provide an electric contact between ITO electrodes and the potentiostat. For the experiments we used following solutions: 10 mM $K_3Fe(CN)_6$ in 0.1 M KCl, 10 mM $K_4Fe(CN)_6$ in 0.1 M KCl, 1 mM dopamine (DA) in 0.1 M phosphate buffered saline solution (PBS) and 2 mM DA in 0.1 M PBS. For the preparation of solutions, we used: KCl and $K_4Fe(CN)_6 \times 3H_2O$ from POCh (pure p.a.), 98% FcDM from ACROS Organics, $K_3Fe(CN)_6$, DA hydrochloride, and PBS tablets from Sigma-Aldrich, and deionized water from a Millipore system. For controlling the flow rate, a Harvard Apparatus Syringe infusion pump 11 equipped with silicone tubing (inner diam. 0.8 μm) was used to pump solutions into the microchannel. For the flow injection experiments an injection valve (Cheminert, Vici) with two different sample loops were used, with lengths 20 and 50 cm. These have an injection volume of 100 μl and 250 μl, respectively. The flow rate was set to 100 μl/min, which is the highest value that ensures that the concentration in the microchannel reaches the same value as in the sample loop (Fig. S2). For EC measurements the flow rate was 5–10 μl/min. The combined EC-optical setup used for measurements is shown in Fig. 1.

2.4. Numerical analysis

Numerical analysis of the flow was performed using the Comsol 5.6 software with the laminar flow module. The EC response was modelled using the electrochemistry module (see Supplementary Information for details), where the electrode reaction was modelled using the Butler-Volmer equation with the exchange current density following the mass action law [39]. The rectangular channel, cavity and electrode geometries were described in 3D coordinates and the change in concentration of the oxidized form of the redox probe during the experiment was monitored as the average at the bottom of the cavity. The Taylor dispersion in the injection loop was simulated in a separate 2D cylindrically symmetrical model with a 10 cm connection tube after the loop. The output concentration from the connection tube was used as input into the microchannel. The angle of the cavity in the flow channel was varied to see the effect on the response time. To investigate the response of the cavity to EC reaction in the channel, we simulated the oxidation of a generic redox probe at an 8 mm wide electrode 1 mm upstream from the fiber. The concentration of the oxidized form at the bottom of the cavity was monitored as a proxy for the optical response. The EC reaction was simulated chronoamperometrically as a potential step to large overpotential and a reverse step after 15 s. The simulation was performed for flowrates from 2 to 25 μl/min for the electrochemical system and 25–250 μl/min for the flow injection system.

3. Results and discussion

3.1. Refractive index sensing

The effect of changes of refractive index in the microcavity for standard conditions without flow channel, where the liquid is exchanged manually using a pipette, is shown in Fig. 2(A). When the RI increases

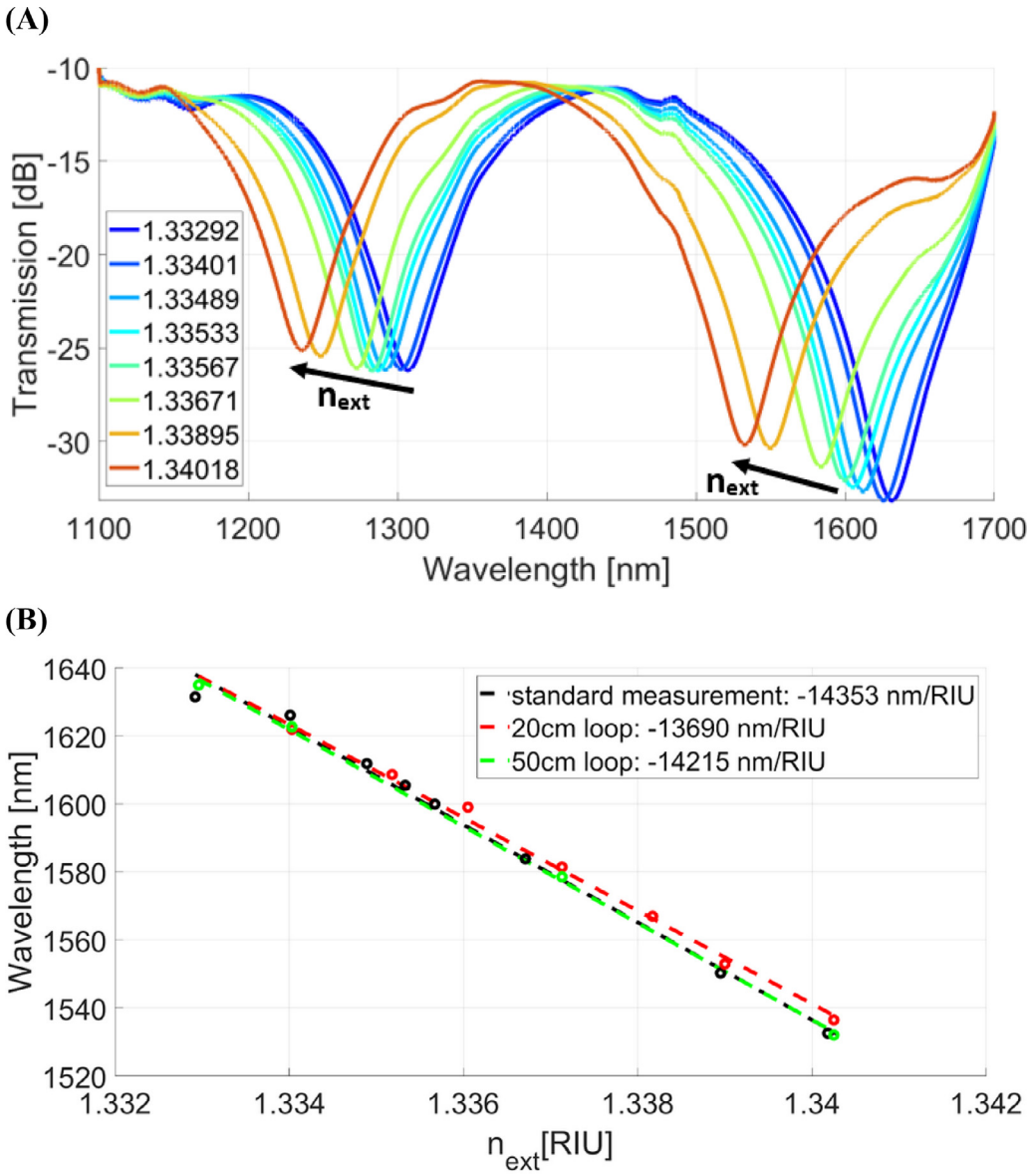

Fig. 2. (A) Transmission spectra of μIMZI filled with next ranging from 1.33292 to 1.34018 RIU and (B) shows corresponding minimum wavelength plotted vs n_{ext} in three different measurement setups: static (standard) measurement, and dynamic measurements using 20 cm and 50 cm long loop.

the minima shift towards shorter wavelengths and reduce their transmission. The phenomenon is originated by the change in guiding conditions of the mode propagating in the cavity and interference at the distant cavity wall [34]. The RI sensitivity of the fabricated μIMZI measured in standard and microfluidic conditions has been compared in Fig. 2(B). It can be seen that for the longer loop applied, i.e., longer exposure to the elevated n_{ext}, the performance of the device is similar to the one at standard conditions, while for the shorter loop, it is slightly lower. The results indicate that exchange of the liquid in the microcavity at the microfluidic conditions requires a certain amount of liquid for the concentration to change completely in the whole cavity volume.

The impact of the exposure of the cavity to liquid of the different n_{ext}, where in this experiment exposure has been set by the length of the loop, is shown in Fig. 3. Experimental data and numerical analysis agree well. The refractive index of the liquid in the loop was 1.34025 RIU while that of the background liquid was 1.33296 RIU. Due to Taylor dispersion in the connection tube, the liquid in the sample loop is slightly diluted and the simulations show that the ultimate concentration (and thus RI) reaches only 85% of its full value for the smaller volume loop. Taylor dispersion is the process through which the difference in flow velocity along the radial direction of the tube leads to a smearing out of the concentration distribution along the direction of the flow [40]. When the concentration/RI of the liquid coming from the loop increases, the wavelength corresponding to the transmission minimum follows and its value decreases. For the shorter loop, in agreement with the simulations, the shift in resonance wavelength is only about 85% of the value for the longer loop.

It was noted, that on top of volume of the exchanged liquid discussed above, also orientation of the cavity versus the flow direction could potentially be a factor influencing the effectiveness of the exchange. Thus, we have performed a numerical analysis aiming to identify the impact of the cavity placement in the microfluidic system. The results are shown in Fig. S2 and S3 of the Supplementary Information and indicate negligible influence of the cavity orientation vs direction of the flow on the exchange of liquid within the timescale of the experiments. The flow rate has a large influence on the final concentration in the channel. For flow rates above 100 μl/min the ultimate concentration is less than the one in the sample loop (Fig. S2), therefore experiments

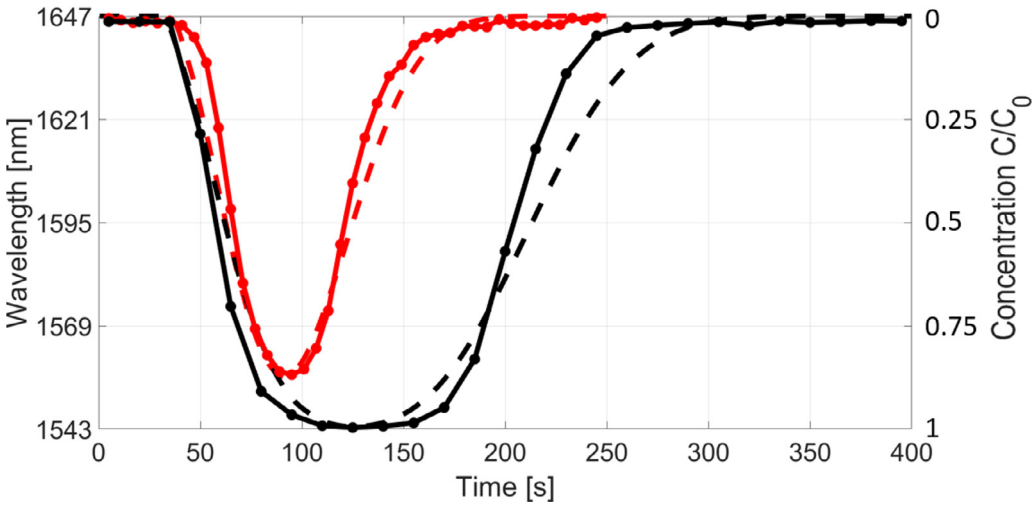

Fig. 3. Concentration profiles, comparing the 20 cm loop (red lines) and the 50 cm loop (black lines). Numerical results are marked with dash lines, experimental results are marked with solid lines. In both cases the n_{ext} change was in the range 1.33296 to 1.34025 RIU. The simulations and the experiments were done for flow rate 100 µl/min.

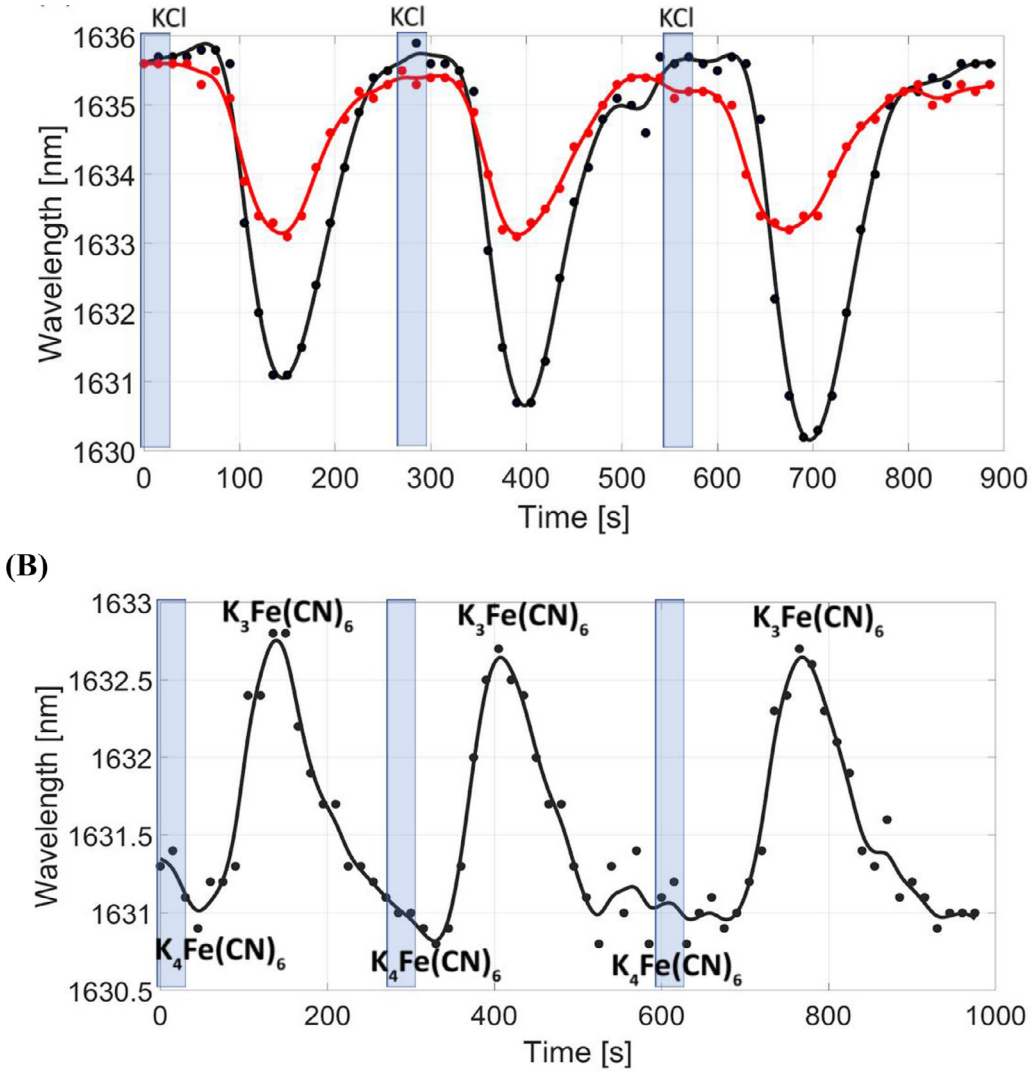

Fig. 4. (A) Wavelength shift in time during exchange 0.1 M KCl (n_D = 1.33409 RIU) to 10 mM $K_4Fe(CN)_6$ in 0.1 M KCl (n_D = 1.33437 RIU) (black line) and during exchange 0.1 M KCl to 10 mM $K_3Fe(CN)_6$ in 0,1 M KCl (n_D = 1.33424 RIU) (red line). (B) Wavelength shifts in time during exchange of 10 mM $K_4Fe(CN)_6$ in 0,1 M KCl (n_D = 1.33437 RIU) to 10 mM $K_3Fe(CN)_6$ in 0,1 M KCl (n_D = 1.33424 RIU). Both in (A) and (B) the exchange of liquids was repeated three times in a 50 cm loop. Blue areas indicate the approximate moment of switching between fluids.

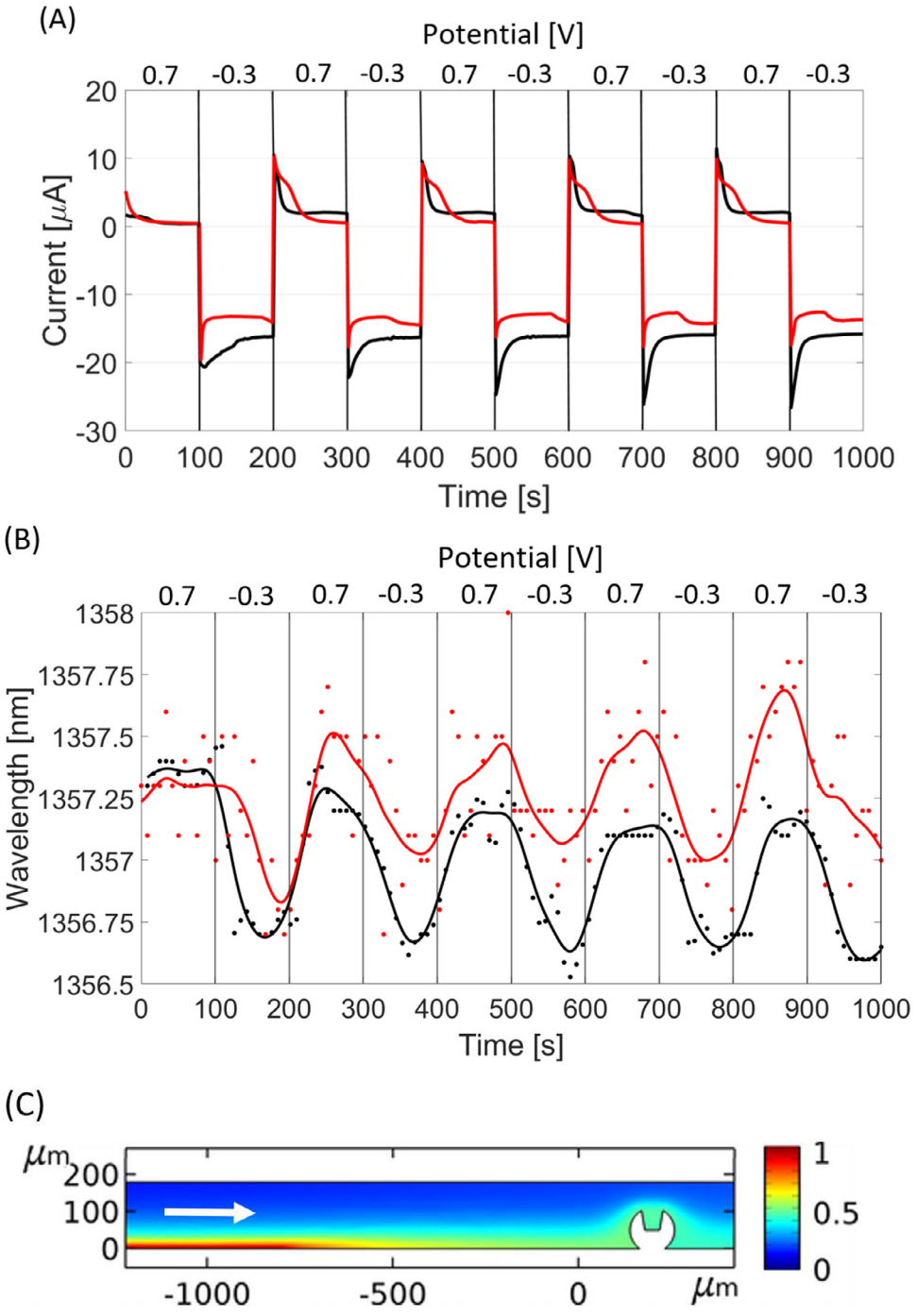

Fig. 5. Current (A) and wavelength (B) shift in time during CA of 10 mM $K_3Fe(CN)_6$ in 0.1 M KCl for different flow speeds: 10 μL/min and 2 μL/min (black and red solid lines, respectively). The lines are a spline fit to the experimental data. (C) shows the simulated concentration profile of the product of the EC reaction at the band working electrode at t = 15 s in a cross-section through the center of the channel for V_f=10 μL/min. The white arrow indicates the flow direction.

were performed using this flow rate to limit the time needed for the measurements.

Next, oxidized and reduced forms of a common redox probe in KCl, as well as KCl as a base electrolyte, were used as liquids flushing the cavity in the microsystem. It can be seen in Fig. 4(A) that when any of the probes is introduced to the supporting electrolyte, the wavelength corresponding to the transmission minimum decreases, but it decreases more (by about 2 nm) when $K_4Fe(CN)_6$ is applied. $K_4Fe(CN)_6$ has a higher RI than the one of $K_3Fe(CN)_6$. A slight increase in the drop with exchange sessions can be seen for $K_4Fe(CN)_6$. This correspond to a sensitivity of about 500 nm/mol for $K_4Fe(CN)_6$ and 300 nm/mol for $K_3Fe(CN)_6$. The exchange between the two forms shown in Fig. 4(B) correspond well with these results and here also wavelength shift reaching about 2 nm can be noticed.

3.2. Monitoring of electrochemical processing

Following the reported above results, the oxidation and reduction of the redox probe was performed directly in the microfluidic channel using the integrated electrodes and a chronoamperometric configuration of the EC setup. The potential applied to the WE was switched between +0.7 and −0.3 V every 100 s. The value +0.7 V is well above the redox potential of the $Fe(CN)_6^{4-/3-}$ couple and −0.3 V well below it, which initializes the reduction of the redox probe, i.e., conversion of $Fe(CN)_6^{3-}$ to $Fe(CN)_6^{4-}$, which gives a negative current. The impact of changes in the applied potential to electrical (Fig. 5(A)) and optical properties (Fig. 5(B)) can be seen at different flow rates. Decrease of E is followed by current and wavelength in EC and optical setup, respectively. While the current between the stages differs by over 15 μA, the

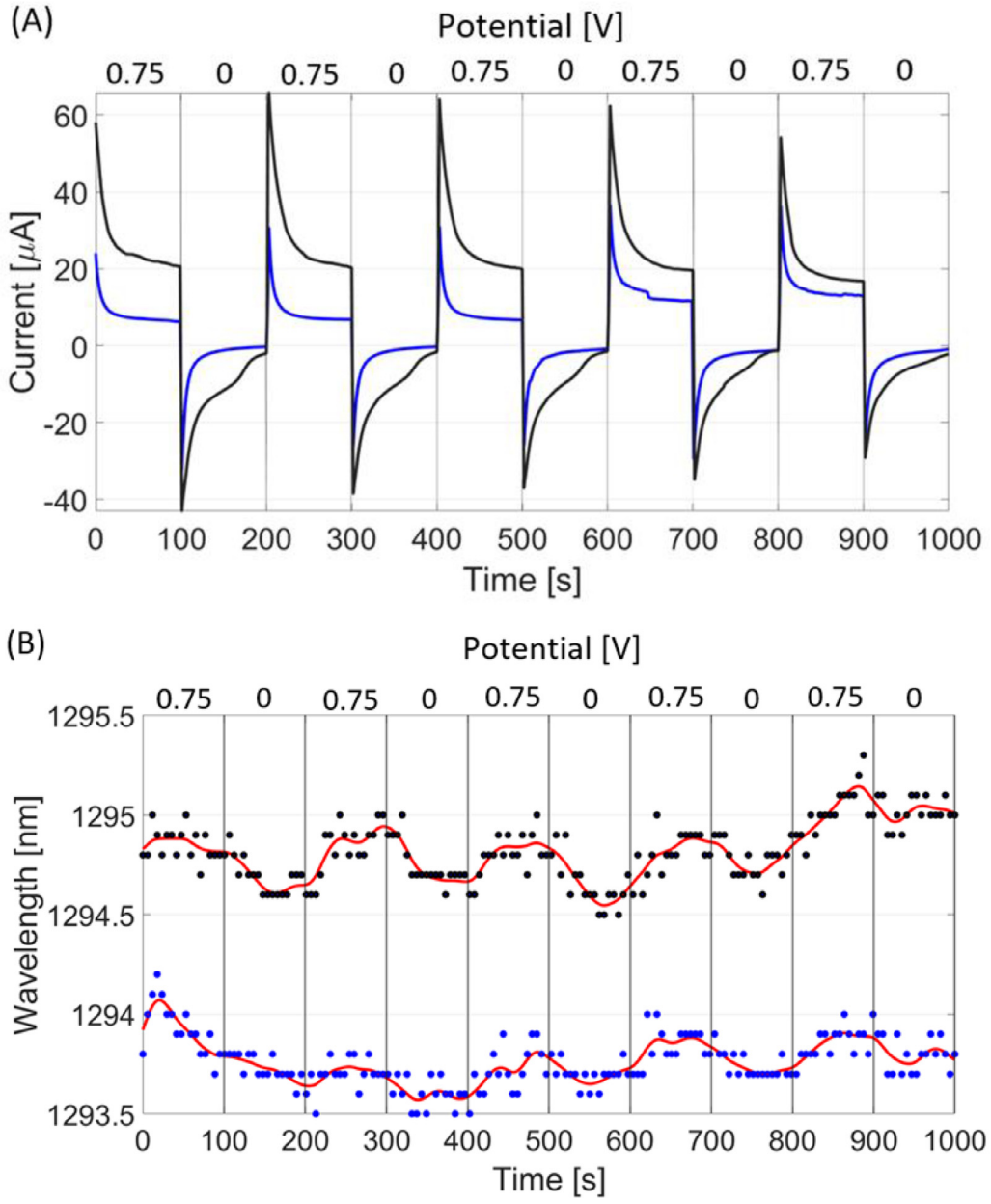

Fig. 6. (A) Current and wavelength (B) shift in time during CA for different DA concentrations: 1 mM (blue), 2 mM (black). Red lines represent fitting functions. Flow rate: 2 μL/min.

wavelength shifts by about 0.7 nm, which is significantly lower than when oxidized and reduced forms of the probe were supplied through the flow injection loop (Fig. 4(B)). This is in relatively good agreement with the simulations that show that for a flow rate of 10 μl/min the concentration of oxidized form of the redox probe reaches about 45% of the concentration of the reduced form in the incoming liquid (Fig. S4), whereas the sensitivity measured from Fig. 4 corresponds to a 35% proportion of the reduced form in the cavity $Fe(CN)_6^{4-}$. The reason is that in the EC experiments the oxidized form is created only at the bottom of the channel (Fig. 5C), while in the flow injection the channel is filled homogeneously with the injected sample. This difference also means that in the EC setup, the response is quite sensitive to the detailed flow of the liquid around the fiber, which can explain why the experimental data correspond less well to the simulation in case of EC actuation as compared to the flow injection. When different flowrates are applied, a clear difference is seen in the current response, but the optical response is quite similar in both cases. In contrast to the simulations, the response at low flowrate is even smaller than for the higher flow. At very low flow rates effects not considered in the simulations, such as convection due to temperature differences in the system, will be more pronounced than when the forced convective flow is higher. This might explain the discrepancy between the simulated and experimental data.

3.3. Monitoring of dopamine

Finally, DA was used in the same EC configuration as for the redox probe discussed in Section 3.2. The results of the measurements are shown in Fig. 6. In this case *E* was switched between 0 and 0.75 V to step from the reduced to the oxidised form of DA. Also in this case we can see that both electrical and optical properties of the DA solution are influenced by *E*. While the current changes more than in case of the probe applied above, the optical subsystem responses weaker than for the redox probe. The wavelength shift for the higher DA concentration reaches

only 0.5 nm. The difference originates from the smaller concentration of DA that can be dissolved in water. If taking into account the level of exchange of in the case of $Fe(Cn)_6^{3-/4-}$ the sensitivity comes to about 350 nm/mol. As in the case for the redox molecule, this corresponds to the difference in optical properties between the reactant and the product. While DA has been measured with very high sensitivity on fiber optical sensors, especially using SPR, this has always been on functionalised sensor surfaces [41–44]. Here, to the best of our knowledge, we show for the first time the measurements on an unfunctionalized sensor surface in combination with electrochemical processing. Despite relatively low optical response, results of EC allows for clear identification of change in the DA concentration. Thus, the combined optical and EC analysis may be treated as complementary. This is a particularly powerful technique if used for monitoring of electrochemical reactions (such as electrocatalysis) in small volume microfluidic systems.

4. Conclusions

Highly functional microfluidic systems need to be supported by subsystems making it possible to efficiently analyze properties of liquids flowing in the microchannel. In this work we have shown both numerical and experimental analysis of microcavity in-line Mach-Zehnder Interferometer (μIMZI) induced in the side surface of a single-mode optical fiber and a microfluidic system. First, it must be noted that after the integration μIMZI maintains its high sensitivity to refractive index changes in the cavity. Second, the amount of liquid flowing in the microchannel and the flow rate need to be adjusted to effectively exchange the liquid in the microcavity, but orientation of the cavity versus the flow direction has a minor impact on the exchange. Finally, we additionally integrated electrodes with the system making it possible to initiate reduction and oxidation reactions directly in the microchannel. It has been shown for a standard redox probe as well as for dopamine that even when the oxidized or reduced form is created in part of the channel, the products of the reactions can be identified both electrochemically and optically. The finding indicates the capability to modify the properties of the liquids outside the microcavity and thanks to the microfluidic system analyze them in the flow. This opens exciting possibilities for monitoring of reactions in microchannels in e.g. electrosynthesis. Moreover, the readouts received in the two domains may deliver more information about the analyte than when investigated separately in each of the domains. There are many opportunities for improvements to follow in the presented microfluidic system. From the optical side of view, increasing the sensitivity of the structures may enable the detection of electrochemical changes in lower concentrations. The circular shape of the microcavity is not the only way to achieve μIMZI. Reshaping the microcavity could allow faster solution exchange, ensuring faster and more reliable measurements. From the electrochemical side, integration of 3D or flow through electrodes or a serpentine path over the working electrode to ensure higher capture efficiency could increase both the processing efficiency and the sensitivity. The results allow for considering the developed system as a promising and universal solution for highly sensitive biochemical analysis in the microscale.

Declaration of Competing Interest

There are no conflicts to declare.

CRediT authorship contribution statement

Andrzej Krześniak: Investigation, Writing – original draft. **Tomasz Gabler:** Investigation, Writing – original draft. **Monika Janik:** Methodology, Writing – original draft. **Marcin Koba:** Methodology, Formal analysis, Writing – review & editing. **Martin Jönsson-Niedziółka:** Conceptualization, Methodology, Investigation, Supervision, Software, Writing – original draft. **Mateusz Śmietana:** Conceptualization, Methodology, Supervision, Writing – original draft, Funding acquisition.

Acknowledgments

This work was supported in Poland by the National Science centre (NCN) under Grant No. NCN 2018/29/B/ST7/02552.

Supplementary materials

Supplementary material associated with this article can be found, in the online version, at doi:10.1016/j.optlaseng.2022.107173.

References

[1] Whitesides GM. The origins and the future of microfluidics. Nature 2006;442:368–73. doi:10.1038/nature05058.
[2] Chiu DT, deMello AJ, Di Carlo D, Doyle PS, Hansen C, Maceiczyk RM, Wootton RCR. Small but perfectly formed? successes, challenges, and opportunities for microfluidics in the chemical and biological sciences. Chem 2017;2:201–23. doi:10.1016/j.chempr.2017.01.009.
[3] Rozniecka E, Jonsson-Niedziolka M, Celebanska A, Niedziolka-Jonsson J, Opallo M. Selective electrochemical detection of dopamine in a microfluidic channel on carbon nanoparticulate electrodes. Analyst 2014;139:2896. doi:10.1039/c3an02207b.
[4] Huang SH, Chang YS, Juang JMJ, Chang KW, Tsai MH, Lu TP, Lai LC, Chuang EY, Huang NT. An automated microfluidic DNA microarray platform for genetic variant detection in inherited arrhythmic diseases. Analyst 2018;143:1367–77. doi:10.1039/c7an01648d.
[5] Zhao SP, Ma Y, Lou Q, Zhu H, Yang B, Fang Q. Three-dimensional cell culture and drug testing in a microfluidic sidewall-attached droplet array. Anal. Chem. 2017;89:10153–7. doi:10.1021/acs.analchem.7b02267.
[6] Wang S, Ai Z, Zhang Z, Tang M, Zhang N, Liu F, Han G, Hong SL, Liu K. Simultaneous and automated detection of influenza a virus hemagglutinin H7 and H9 based on magnetism and size mediated microfluidic chip. Sens. Actuators B Chem. 2020;308:127675. doi:10.1016/j.snb.2020.127675.
[7] Monat C, Domachuk P, Eggleton BJ. Integrated optofluidics: a new river of light. Nat. Photonics 2007;1:106–14. doi:10.1038/nphoton.2006.96.
[8] Ozcelik D, Cai H, Leake KD, Hawkins AR, Schmidt H. Optofluidic bioanalysis: fundamentals and applications. Nanophotonics 2017;6:647–61. doi:10.1515/nanoph-2016-0156.
[9] Butement JT, Hunt HC, Rowe DJ, Minzioni P, Osellame R, Sada C, Zhao S. Roadmap for optofluidics. J. Opt. 2017;19:93003.
[10] Song C, Tan SH. A perspective on the rise of optofluidics and the future. Micromachines 2017;8:1–17 (Basel). doi:10.3390/mi8050152.
[11] Bates KE, Lu H. Biophysical perspective optics-integrated microfluidic platforms for biomolecular analyses. Biophys. J. 2016;110:1684–97. doi:10.1016/j.bpj.2016.03.018.
[12] Barshilia D, Chau LK, Chang GE. Low-cost planar waveguide-based optofluidic sensor for real-time refractive index sensing. Opt. Express 2020;28:27337–45.
[13] Zhao Y, guang Hu X, Hu S, Peng Y. Applications of fiber-optic biochemical sensor in microfluidic chips: a review. Biosens. Bioelectron. 2020;166:112447. doi:10.1016/j.bios.2020.112447.
[14] Pissadakis S. Lab-in-a-fiber sensors: a review. Microelectron. Eng. 2019;217:1–21. doi:10.1016/j.mee.2019.111105.
[15] Blue R, Duduś A, Uttamchandani D. A review of single-mode fiber optofluidics. IEEE J. Sel. Top. Quantum Electron. 2016;22:380–91. doi:10.1109/JSTQE.2015.2466071.
[16] Li L, nan Zhang Y, Zhou Y, Zheng W, Sun Y, Ma G, Zhao Y. Optical fiber optofluidic bio-chemical sensors: a review. Laser Photonics Rev. 2021;15:1–56. doi:10.1002/lpor.202000526.
[17] Shao L, Liu Z, Hu J, Gunawardena D, Tam HY. Optofluidics in microstructured optical fibers. Micromachines 2018;9:1–19 (Basel). doi:10.3390/mi9040145.
[18] Gao R, Lu DF, Zhang MY, Qi ZM. Optofluidic immunosensor based on resonant wavelength shift of a hollow core fiber for ultratrace detection of carcinogenic benzo[a]pyrene. ACS Photonics 2018;5:1273–80. doi:10.1021/acsphotonics.7b01009.
[19] Sugioka K, Cheng Y. Femtosecond laser processing for optofluidic fabrication. Lab. Chip. 2012;12:3576–89. doi:10.1039/c2lc40366h.
[20] Haque M, Lee KKC, Ho S, Fernandes LA, Herman PR. Chemical-assisted femtosecond laser writing of lab-in-fibers. Lab. Chip. 2014;14:3817–29. doi:10.1039/c4lc00648h.
[21] Zhang D, Wei H, Krishnaswamy S. 3D printing optofluidic Mach-Zehnder interferometer on a fiber tip for refractive index sensing. IEEE Photonics Technol. Lett. 2019;31:1725–8. doi:10.1109/LPT.2019.2943897.
[22] Lee SM, Jeong MY, Saini SS. Etched-core fiber Bragg grating sensors integrated with microfluidic channels. J. Light. Technol. 2012;30:1025–31. doi:10.1109/JLT.2011.2167220.
[23] Jiang B, Dai H, Zou Y, Chen X. Continuous detection of micro-particles by fiber Bragg grating Fabry-Pérot flow cytometer. Opt. Express 2018;26:12579. doi:10.1364/oe.26.012579.
[24] Murib MS, Martens D, Bienstman P. Label-free real-time optical monitoring of DNA hybridization using SiN Mach–Zehnder interferometer-based integrated biosensing platform. J. Biomed. Opt. 2018;23:1. doi:10.1117/1.jbo.23.12.127002.
[25] Yan SC, Xu F. A review on optical microfibers in fluidic applications. J. Micromech. Microeng. 2017;27:1–20. doi:10.1088/1361-6439/aa7a45.
[26] Liang L, Zhao C, Xie F, Sun LP, Ran Y, Jin L, Guan BO. Sensitivity enhancement of a fiber-based interferometric optofluidic sensor. Opt. Express. 2020;28:24408. doi:10.1364/oe.400325.

[27] Yang Y, Bandyopadhyay S, Shao L, Jiang J, Peng Z, Liu S, Hu J, Shum PP, Hu J, Zhang X. Anomalous sensitivity enhancement of d-shaped fiber-based sandwiched structure Optofluidic sensor. IEEE Access 2020;8:105207–16. doi:10.1109/ACCESS.2020.2999733.

[28] Chiavaioli F, Zubiate P, Del Villar I, Zamarrenìo CR, Giannetti A, Tombelli S, Trono C, Arregui FJ, Matias IR, Baldini F. Femtomolar detection by nanocoated fiber label-free biosensors. ACS Sens. 2018;3:936–43. doi:10.1021/acssensors.7b00918.

[29] Yin M, Huang B, Gao S, Zhang AP, Ye X. Optical fiber LPG biosensor integrated microfluidic chip for ultrasensitive glucose detection. Biomed. Opt. Express 2016;7:2067. doi:10.1364/boe.7.002067.

[30] Janik M, Myśliwiec AK, Koba M, Celebańska A, Bock WJ, Śmietana M. Sensitivity pattern of femtosecond laser Mach-Zehnder interferometers, as applied to small-scale refractive index sensing. IEEE Sens. J. 2017;17:3316–22.

[31] Janik M, Member S, Eftimov T, Koba M, Smietana M, Bock WJ, Member L. Tailoring properties of microcavity in-line Mach-Zehnder interferometer by the microcavity enlargement using femtosecond laser. J. Light Technol. 2019;37:4501–6. doi:10.1109/JLT.2019.2907661.

[32] Janik M, Brzozowska E, Czyszczoń P, Celebańska A, Koba M, Gamian A, Bock WJ, Śmietana M. Optical fiber aptasensor for label-free bacteria detection in small volumes. Sens. Actuators B Chem. 2021;330:1–10. doi:10.1016/j.snb.2020.129316.

[33] Janik M, Koba M, Celebańska A, Bock WJ, Śmietana M, Live E. coli bacteria label-free sensing using a microcavity in-line Mach-Zehnder interferometer. Sci. Rep. 2018;8:1–8. doi:10.1038/s41598-018-35647-2.

[34] Janik M, Hamidi SV, Koba M, Perreault J, Walsh R, Bock WJ, Śmietana M. Real-time isothermal DNA amplification monitoring in picoliter volumes using an optical fiber sensor. Lab. Chip. 2021;21:397–404. doi:10.1039/D0LC01069C.

[35] Janczuk-Richter M, Dominik M, Koba M, Mikulic P, Bock WJ, MacKowski S, Jonsson-Niedziolka M, Niedziolka-Jonsson J, Smietana M. Water-induced fused silica glass surface alterations monitored using long-period fiber gratings. J. Lights Technol. 2019:37. doi:10.1109/JLT.2019.2909947.

[36] Li Z, Liao C, Chen D, Song J, Jin W, Peng GD, Zhu F, Wang Y, He J, Wang Y. Label-free detection of bovine serum albumin based on an in-fiber Mach-Zehnder interferometric biosensor. Opt. Express 2017;25:17105. doi:10.1364/OE.25.017105.

[37] Gabler T, Krześniak A, Janik M, Myśliwiec A, Koba M, Buczyńska J, Jönsson-Niedziółka M, Śmietana M. Electrochemistry in an optical fiber microcavity – optical monitoring of electrochemical processes in picoliter volumes. Lab Chip 2021;21:2763–70. doi:10.1039/D1LC00324K.

[38] Qiu J, Miura K, Hirao K. Femtosecond laser-induced microfeatures in glasses and their applications. J. Non-Cryst. Solids 2008;354:1100–11. doi:10.1016/j.jnoncrysol.2007.02.092.

[39] Dickinson EJF, Wain AJ. The Butler-Volmer equation in electrochemical theory: origins, value, and practical application. J. Electroanal. Chem. 2020;872:114145. doi:10.1016/j.jelechem.2020.114145.

[40] Taylor GI. Dispersion of soluble matter in solvent flowing slowly through a tube. Proc. R. Soc. Lond. Ser. Math. Phys. Sci. 1953;219:186–203. doi:10.1098/rspa.1953.0139.

[41] Rithesh Raj D, Prasanth S, Sudarsanakumar C. Development of LSPR-based optical fiber dopamine sensor using l-tyrosine-capped silver nanoparticles and its nonlinear optical properties. Plasmonics 2017;12:1227–34. doi:10.1007/s11468-016-0380-5.

[42] Kamal Eddin FB, Fen YW, Omar NAS, Liew JYC, Daniyal WMEMM. Femtomolar detection of dopamine using surface plasmon resonance sensor based on chitosan/graphene quantum dots thin film. Spectrochim. Acta Part Mol. Biomol. Spectrosc. 2021;263:120202. doi:10.1016/j.saa.2021.120202.

[43] Pathak A, Gupta BD. Ultra-selective fiber optic SPR platform for the sensing of dopamine in synthetic cerebrospinal fluid incorporating permselective nafion membrane and surface imprinted MWCNTs-PPy matrix. Biosens. Bioelectron. 2019;133:205–14. doi:10.1016/j.bios.2019.03.023.

[44] Janik M, Janczuk-Richter M, Burnat D, Gabler T, Niedziółka-Jönsson J, Koba M, Sezemsky P, Stranak V, Śmietana M. Dopamine sensing with electrochemically-enhanced ITO-coated lossy-mode resonance optical fiber sensor. In: Proceedings of the Optical Fiber Sensors Conference 2020 Special Edition, OSA, Washington, D.C.; 2021. Th4.18.